Coupled Defects in Photonic Crystals

Andrew L. Reynolds, Ulf Peschel, Falk Lederer, Peter John Roberts, Thomas F. Krauss, and Peter J. I. de Maagt, *Member, IEEE*

***Abstract*—We present a theoretical and numerical description of coupled defects in photonic-bandgap crystals, expandable to cover a wide range of applications. Based on a weak interaction approach, explicit expressions are derived for defect interaction. The basis is formed by a system of coupled ordinary differential equations for the field amplitudes for individual defects. The actual configuration of the defects (chain, lattice, bend, or anything else) enters the equations as a linear coupling between neighboring defects. The strength of this method is that many solutions of this system are known analytically; the band structure as well as the transmission response of a defect chain, or of a defect lattice, can be determined. The results for the superlattice of defects are compared with widely accepted numerical methods, the transfer matrix method, and finite-difference time domain.**

***Index Terms*—Electromagnetic crystals, periodic structures, photonic-bandgap crystals.**

I. Introduction

AN IDEAL photonic crystal (PC) is constructed by the infinite repetition of identical structural units in space. With correct design, this affords us control over the emission and propagation of electromagnetic waves through resultant gaps in the dispersion relation, the photonic bandgaps (PBG). Considerable effort in theoretical, experimental and material fabrication research has predicted and demonstrated many of the properties of these ideal crystals. By placing a "defect unit" within an otherwise perfect PC a localized resonance peak in transmission may be created within the forbidden bandgap of the structure. Introducing further defects into the crystal and placing them within coupling distance opens up a miniband of allowed transmission [1], [2].

Chains of defects form a mechanism for waveguiding, commonly referred to as coupled-cavity waveguides (CCW), and can be used to make wavelength selective efficient waveguides, bends and splitters [3]–[7]. The spectral properties of such waveguides are determined by the nature of the defects and their spacing; both broad-band and narrow-band waveguides can be created. While defects within planar PCs may also be used to increase light emission [8], this paper examines the effects of proximity between defects on waveguiding.

For the hexagonal lattice studied, two incidence directions were studied and the width and miniband localization frequency are investigated as a function of coupling distance between defects within the lattice. Crosstalk minimization or defect isolation is achieved at a much faster rate than was at first expected. The CCW system is created by introducing a similar geometry superlattice of defects into a fundamental hexagonal lattice of air holes in dielectric. Defects can be introduced by altering the size of one or more of the constituent features of the lattice, in our case by completely in-filling the air holes at superlattice sites.

Previous work has examined defects within PCs forming efficient bends and waveguides [9]–[11]. Tayeb examined the influence of more than one localized defect as a function of distance [12]. We distinguish our coupled-cavity analysis from that of the continuous dielectric PC waveguides as rigorously examined, for example by Sondergaard and Dridi [13] and Yonekura *et al.* [14].

II. Lattice Definitions

The fundamental lattice consists a hexagonal array of air holes introduced into a dispersionless bulk refractive index material $n_{\mathrm{material}} = 2.81$ ($\varepsilon_r = 7.9$), figures representative of the effective index of a GaAs waveguide that is $\lambda/2$ thick and that has oxidized AlGaAs on one side and air on the other. The air cylinders were chosen to have a ratio of radius, r, to lattice constant, a, of $r/a = 0.35$. Analysis of the perfect lattice confirmed a gap region for TE polarized waves between normalized frequencies of approximately $a/\lambda = 0.235$–0.37 for ΓM incidence, and 0.27–0.41 for ΓK, see Fig. 1 for incidence orientations. In this range, TM polarized waves do not display PBG behavior.

III. Coupled–Mode Theory for Coupled–Defect Systems

In this section a coupled-mode theory is developed and the results based on this approximation are compared with the response of the coupled-defect lattice determined with the transfer matrix method. This approach provides as with a deeper insight into the energy transfer dynamics of coupled-defect systems.

A. The Model

In case of weak interaction the modal field structure of individual defects remains unchanged, only the respective field amplitudes evolve in time. Provided that the individual defects are similar and single mode, the dynamics of the coupled-defect

Manuscript received January 4, 2001; revised May 23, 2001.

A. L. Reynolds was with the University of Glasgow, Glasgow, G12 8LT, Scotland. He is now with Harlow Laboratories, Nortel Networks, Harlow, Essex CM17 9NA, U.K.

U. Peschel and F. Lederer are with the Friedrich-Schiller-Universität Jena, 07743 Jena, Germany.

P. J. Roberts is with the Defence Evaluation Research Agency, DERA Malvern, Malvern, WR14 3PS, U.K.

T. F. Krauss is with the School of Physics and Astronomy, University of St. Andrews, St. Andrews, Fife KY16 9SS, Scotland.

P. J. I. de Maagt is with the Electromagnetics Division, European Space Research and Technology Centre, 2201 AG Noordwijk, The Netherlands (e-mail: Peter.de.Maagt@esa.int).

Publisher Item Identifier S 0018-9480(01)08729-4.

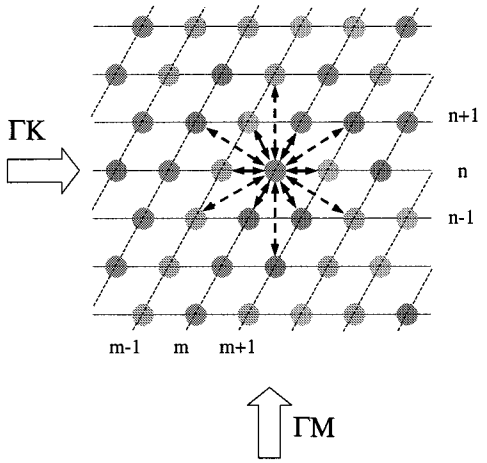

Fig. 1. Interaction and notation for the superlattice of coupled defects. ΓM/ΓK-directions [full line with arrow: nearest neighbor interaction (coefficient c_0), dashed line with arrow: next nearest neighbor interaction (coefficient c_1)]. Note that for the ΓK-direction the m and n labels should be switched for consistency with the text.

system are described by a set of ordinary differential equations, given generally by [1] (see the Appendix):

$$i\frac{d}{dt}a_i = (\omega_0 - i\gamma_i)a_i - \sum_{\substack{j=1\\ j\neq i}}^{N} c_{ij}a_j + \hat{\tau}_i a_{\mathrm{in}_i} \tag{1}$$

where the sum is the energy transfer between the N defect modes, ω_0 is the eigenfrequency of the defect, and γ_i is the decay rate of the effect. In this section, a perfect crystal is assumed, i.e., dielectric losses are assumed to be negligible. Hence, all damping is solely due to power transfer to the environment of the crystal. Obviously, γ_i is different from zero for defects close to the side facet of the crystal as it is for the driving field at the defect a_{in_i} that couples to the outermost defects via $\hat{\tau}_i$. Conservation of energy determines the relations between the coupling to external fields and radiative losses [2] (see the Appendix). Therefore, the transmitted field is always proportional to the amplitudes of the defect amplitudes closest to the output facet. The overall dynamical response of the defect system is determined by the coupling coefficients c_{ij}. They are given by the mutual overlap between the field structures of the defect modes $\vec{E}_i$ and $\vec{E}_j$ and the changes of the dielectric constant $\delta\varepsilon_R$, which has induced the defects

$$c_{ij} = \omega_0 \frac{\int d^3r \delta\varepsilon_R \vec{E}_i^* \vec{E}_j}{\int d^3r \varepsilon_{\mathrm{R}} |E_i|^2}. \tag{2}$$

There are more elegant ways to determine the values of the coupling coefficients, however, general principles can be learned from (2). The fields involved are related to nonpropagating modes that possess evanescent tails. As the distance between the defects increases, the coupling efficiency rapidly decays to zero because the overlap between the evanescent tails of the interacting fields decays exponentially. Normally only the interaction between neighboring defects has to be taken into account and if the defect lattice has certain symmetries, most of the coefficients c_{ij} are equal. For our hexagonal lattices a single coefficient, c_0, determines the nearest neighbor interaction, see Fig. 1. The distance to the six next nearest neighbors (coefficient c_1) is already $\sqrt{3}$ times bigger, decreasing the relation between c_1 and c_0 due to the decaying field overlaps. Hence, if the defect spacing is increased further, the interaction will be very weak and it is valid to restrict analysis to nearest neighbor interaction, setting c_1 to zero. Only in case of strong interaction, i.e., for a rather short spacing between the defects, should next nearest neighbor interaction be taken into account. For our hexagonal superlattice of defects, nearest neighbor interaction is by far the most dominant, but next nearest neighbor interaction still has some effect.

To describe the response of the hexagonal defect lattice using plane-wave excitation, a convenient notation is adopted whose structure depends on the direction of excitation.

B. Field Propagation Into the ΓM-Direction

Coupled-mode equations are derived for nearest neighbor interaction, the inclusion of next nearest neighbor interaction ($c_1 \neq 0$) is straightforward and respective results are also presented. By assuming that $c_1 = 0$ only the outermost rows of defects interact with external fields. Hence, any damping or excitation from outside for all defects $1 < n < N$ is neglected. Using the notation from Fig. 1, the following evolution equations for the defect amplitudes is obtained:

$n = 1$:

$$i\frac{d}{dt}a_{1m} = (\omega_0 - i\gamma_1)a_{1m} - c_0(a_{1m-1} + a_{1m+1} + a_{2m} + a_{2m-1}) + \hat{\tau}_1 a_{\mathrm{in}m} \tag{3a}$$

$1 < n < N$:

$$i\frac{d}{dt}a_{nm} = \omega_0 a_{nm} - c_0(a_{nm-1} + a_{nm+1} + a_{n-1m} + a_{n+1m} + a_{n+1m-1} + a_{n-1m+1}) \tag{3b}$$

$n = N$:

$$i\frac{d}{dt}a_{Nm} = (\omega_0 - i\gamma_N)a_{Nm} - c_0(a_{Nm-1} + a_{Nm+1} + a_{N-1m} + a_{N-1m+1}). \tag{3c}$$

The field in the first line is driven by a harmonic excitation

$$a_{\mathrm{in}\,m} = b_{\mathrm{in}} \exp(i\kappa m - i\omega t) \tag{4a}$$

which induces the same harmonic dependence in the whole lattice as

$$a_{nm} = b_n \exp(i\kappa m - i\omega t) \tag{4b}$$

where ω is the frequency of the wave and κ is related to its tilt angle α, the defect spacing L and the index of the host material n_h by

$$\kappa = \sin(\alpha) L n_h \frac{\omega}{c}. \tag{5}$$

Since only the outermost defect rows couple to outer space the transmitted field is strictly proportional to the mode amplitude of the last defects (number N)

$$b_\tau = c_{\tau_N} b_N.$$

Because only a single defect row is assumed to interact with outer space it is possible to derive some explicit relations between the damping constants and the coupling to external radiation as [15]

$$|c_{\tau_N}|^2 = 2\gamma_N \Gamma \tag{6a}$$

$$|\hat{\tau}_1|^2 = 2\frac{\gamma_1}{\Gamma} \tag{6b}$$

where Γ is the lateral defect density. Substitution of (4a) and (4b) into (3a)–(3c) reduces the two-dimensional (2-D) defect lattice into an effective defect chain, which is described by a system of algebraic equations like

$n = 1$:

$$0 = [-\delta\omega - i\gamma_1 - 2c_0\cos(\kappa)]b_1 - c_0[1+\exp(-i\kappa)]b_2 + \hat{\tau}_1 b_{\text{in}} \tag{7a}$$

$1 < n < N$:

$$0 = [-\delta\omega - 2c_0\cos(\kappa)]b_n - c_0[1+\exp(i\kappa)]b_{n-1} - c_0[1+\exp(-i\kappa)]b_{n+1} \tag{7b}$$

$n = N$:

$$0 = [-\delta\omega - i\gamma_N - 2c_0\cos(\kappa)]b_N - c_0[1+\exp(i\kappa)]b_{N-1} \tag{7c}$$

where $\delta\omega = \omega - \omega_0$ is the frequency shift between the defect and the incident wave. The whole system of equations (7a)–(7c) is symmetric with respect to the transformation

$$\delta\omega \Rightarrow -\delta\omega - 4c_0\cos(\kappa) \quad \kappa \Rightarrow -\kappa \quad b_n \Rightarrow (-1)^n b_n^*. \tag{8}$$

With this assumption the frequency response is expected to be symmetric with respect to the defect frequency ω_0 shifted by $-2c_0\cos(\kappa)$. Solutions of the system (7a)–(7c) consist of harmonic waves travelling along the effective chain like

$$b_n = b_+\exp(i\alpha_+ n) + b_-\exp(i\alpha_- n) \tag{9}$$

where α_+ and α_- are given by the two solutions of the dispersion relation, which also defines the band structure of the defect lattice:

$$\delta\omega = -2c_0[\cos(\kappa) + 2\cos(\alpha - \kappa/2)\cos(\kappa/2)]. \tag{10}$$

The amplitudes of the forward and backward propagating waves b_+ and b_-, respectively, can be determined by substituting (9) and (10) into (7a) and (7c). The transmitted field is then given by

$$b_\tau = c_{\tau_N}[b_+\exp(i\alpha_+ N) + b_-\exp(i\alpha_- N)].$$

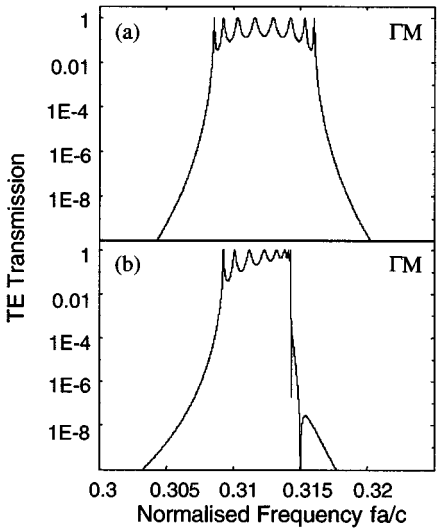

Fig. 2. Transmission of a hexagonal defect lattice along the ΓM-direction. Approximated by a coupled-mode theory (parameters: polarization TE, 1 defect in 3 unit cells, $N = 8$, $c_0 = 0.001$, $\gamma_1 = \gamma_N = 0.0004$, $\gamma_2 = \gamma_{N-1} = 0$, $\hat{\tau}_1 = c_{\tau_N} = \sqrt{2\gamma_1}$, $\hat{\tau}_2 = c_{\tau_{N-1}} = 0$, $\omega_0 = 0.3103$). (a) Nearest neighbor interaction only ($c_1 = 0$). (b) Nearest and next nearest neighbor interaction ($c_1 = c_0/3$).

Therefore the transmission of the whole structure looks like

$$\tau(\kappa, \delta\omega) = \frac{\hat{\tau}_1 c_{\tau_N}\sin\alpha\exp(-iN\varphi)}{\frac{\gamma_1\gamma_N}{c}\sin[\alpha(N-1)] + i(\gamma_1+\gamma_N)\sin(\alpha N) - c\sin[\alpha(N+1)]} \tag{11}$$

where $c\exp(i\varphi) = c_0[1+\exp(-i\kappa)]$ and $\alpha = \arccos((2c_0\cos(\kappa) - \delta\omega)/2c)$. A few interesting things can be learned from (11). First, a limited band of transmission is defined consisting of a series of peaks, all approaching 1 for the case of a symmetric structure [see Fig. 2(a)]. The width of the individual peaks is different, large in the middle of the miniband and small at the edges, confirming that the photon lifetime depends on the excitation frequency. In the middle of the miniband photons travel with maximum speed and leave the structure quickly, where at the edges of the miniband the group velocity approaches zero, a fact confirmed experimentally [5].

The transmission relation (11) is symmetric due to relation (8). By taking into account the next nearest neighbor interaction, coefficient c_1, the asymmetric terms of the spectral response are generated. By following a similar procedure to that above, analytical expressions can be obtained, but the final expressions, which include the solution of a fourth order polynomial to determine α in an expression similar to (11), are much to involved to be reproduced. Fig. 2(b) shows the resultant transmission plot, modeling a 1 in 3 defect lattice. The corresponding values to reproduce these figures are in normalized units: $c_0 = -0.001$, $c_1 = c_0/3$, $\gamma = 0.0004$ and $\omega_0 = 0.3103$. Although the defect spacing is rather large the next nearest neighbor interaction is present and adds important new features, mainly an asymmetric response.

C. Field Propagation into the ΓK-Direction

Interchanging m for n in Fig. 1 and making the same approximations as for the ΓM-direction, the respective evolution equations for field propagation into ΓK direction are

$n = 1$:

$$i\frac{d}{dt}a_{1m} = -c_0(a_{2m} + a_{2m+1} + a_{3m+1}) + \omega_0 a_{1m} - i\gamma a_{1m} + \hat{\tau}_1 a_{\mathrm{in}\,m} \tag{12a}$$

$n = 2$:

$$i\frac{d}{dt}a_{2m} = -c_0(a_{1m-1} + a_{1m} + a_{3m} + a_{3m+1} + a_{4m+1}) + \omega_0 a_{2m} \tag{12b}$$

$2 < n < N - 1$:

$$i\frac{d}{dt}a_{nm} = -c_0(a_{n-2m-1} + a_{n-1m-1} + a_{n-1m} + a_{n+1m} + a_{n+1m+1} + a_{n+2m+1}) + \omega_0 a_{nm} \tag{12c}$$

$n = N - 1$:

$$i\frac{d}{dt}a_{N-1m} = -c_0(a_{N-3m-1} + a_{N-2m-1} + a_{N-2m} + a_{Nm} + a_{Nm+1}) + \omega_0 a_{N-1m} \tag{12d}$$

$n = N$:

$$i\frac{d}{dt}a_{Nm} = -c_0(a_{N-2m-1} + a_{N-1m-1} + a_{N-1m}) + \omega_0 a_{Nm}. \tag{12e}$$

Assuming incidence in the form of (4a) and (4b) reduces (12a)–(12e) to a set of algebraic equations

$n = 1$:

$$0 = -(\delta\omega + i\gamma)b_1 - c_0\{[1 + \exp(i\kappa)]b_2 + \exp(i\kappa)b_3\} + \hat{\tau}_1 b_{\mathrm{in}} \tag{13a}$$

$n = 2$:

$$0 = -\delta\omega b_2 - c_0\{[1 + \exp(-i\kappa)]b_1 + [1 + \exp(i\kappa)]b_3 + \exp(i\kappa)b_4\} \tag{13b}$$

$2 < n < N - 1$:

$$0 = -\delta\omega b_n - c_0\{\exp(-i\kappa)b_{n-2} + [1 + \exp(-i\kappa)]b_{n-1} + [1 + \exp(i\kappa)]b_{n+1} + \exp(i\kappa)b_{n+2}\} \tag{13c}$$

$n = N - 1$:

$$0 = -\delta\omega b_{N-1} - c_0\{\exp(-i\kappa)b_{N-3} + [1 + \exp(-i\kappa)]b_{N-2} + [1 + \exp(i\kappa)]b_N\} \tag{13d}$$

$n = N$:

$$0 = -(\delta\omega + i\gamma)b_N - c_0\{\exp(-i\kappa)b_{N-2} + [1 + \exp(-i\kappa)]b_{N-1}\}. \tag{13e}$$

Although only nearest neighbor interaction has been included in (12a)–(12e) the set of equations (13a)–(13e) describing the effective defect chain already includes terms that spread further. The immediate consequence is the loss of the symmetry as described by (8). Hence, even if next nearest neighbor interaction can be neglected due to large defect spacing an asymmetrical frequency response of the lattice illuminated from the ΓK-direction will be found. Fig. 3 shows two plots of the transmission in ΓK-direction, which are obtained by solving the system of equations (13a)–(13e) and a respective set of equations with next nearest neighbor interaction included, the response is asymmetric. However, the inclusion of next nearest neighbor interaction changes the symmetry, compare Fig. 3(a) and (b). In contrast to the ΓM-direction, for the ΓK-direction it was also necessary to include the free space radiation with the second line of defects. This can be understood by looking at Fig. 1. In case of the ΓK-direction the second line of defects is much closer to a respective interface facet than in case of the ΓM-direction.

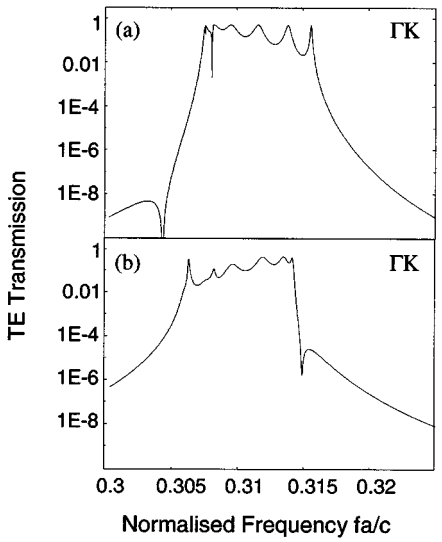

Fig. 3. Transmission of a hexagonal defect lattice along the ΓK-direction. Approximated by a coupled-mode theory (parameters: polarization TE, 1 defect in 3 unit cells, $N = 8$, $c_0 = 0.001$, $\gamma_1 = \gamma_N = 0.0008$, $\hat{\tau}_1 = c_{\tau_N} = \sqrt{\gamma_1/2}$, $\omega_0 = 0.3103$). (a) Nearest neighbor interaction only ($c_1 = 0$, $\gamma_2 = \gamma_{N-1} = 0$, $\hat{\tau}_2 = c_{\tau_{N-1}} = 0$). (b) Nearest and next nearest neighbor interaction ($c_1 = c_0/3$, $\gamma_2 = \gamma_{N-1} = 0.0004$, $\hat{\tau}_2 = c_{\tau_{N-1}} = \sqrt{\gamma_2/2}\exp(-i\pi/2)$).

IV. Transfer Matrix Method Analysis

A modified version of the transfer matrix method as described by Pendry, Bell, and Ward [17]–[22] has been utilized to provide a comparison with the analytical results presented in the previous sections [23]. The conventional cell of the superlattice, assumed in Figs. 4–6, was represented using a 2-D orthogonal Cartesian discretization mesh. A cell is defined as the smallest building block that self-repeats to generate the crystal.

A. Defects: One in Every Three, ΓK and ΓM

Fig. 4 shows the miniband TE polarized transmission response for the ΓM and ΓK propagation directions as an evolution of the number of conventional superlattice cells. Incidence in either lattice direction shows a central miniband normalized frequency of $fa/c = 0.312$, a figure in good agreement with the analytical results presented in Figs. 2 and 3. Compare Fig. 2(b) with Fig. 5 to contrast the analytical and TMM methods. The trend toward this localization frequency is even present for propagation through a single cell. Increasing the number of cells does not alter the localization frequency; see Fig. 4.

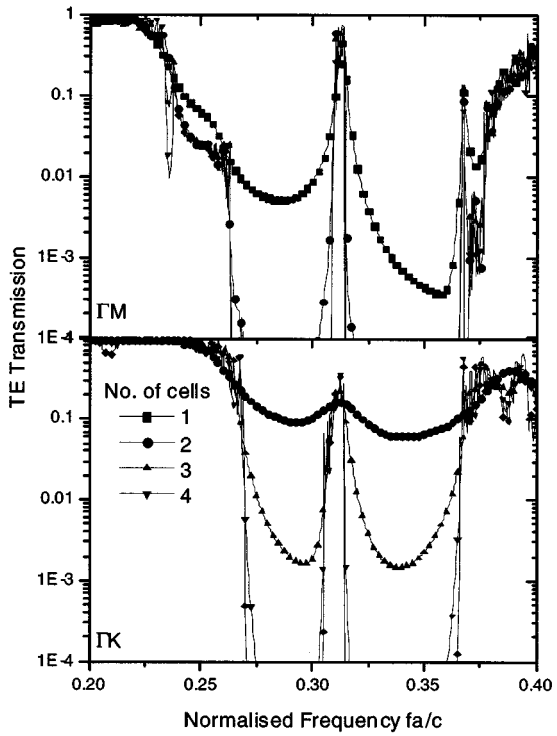

Fig. 4. Periodic Defects: one in every three, ΓM and ΓK. The transmission response of a TE polarized wave as a function of normalized frequency and crystal thickness expressed in terms of the number of cells through which the wave has been propagated. Defects have been introduced periodically along the high symmetry axis of the crystals one in every three lattice spacings. (top): ΓM response. (bottom): ΓK response.

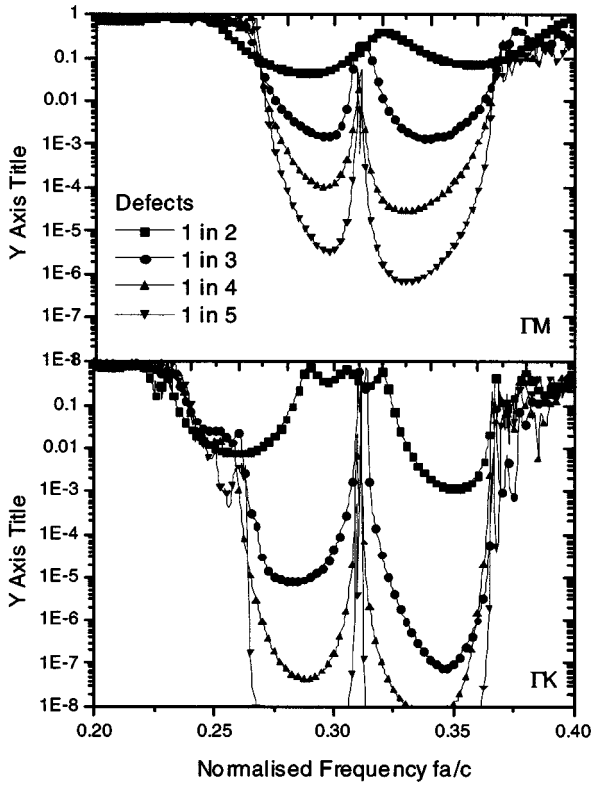

Fig. 6. Evolution for superlattice spacing. The TE polarized wave response against normalized frequency as a function of the neighbor to neighbor defect superlattice spacing for propagation through two cells of structure. (top): ΓM response. (bottom): ΓK response.

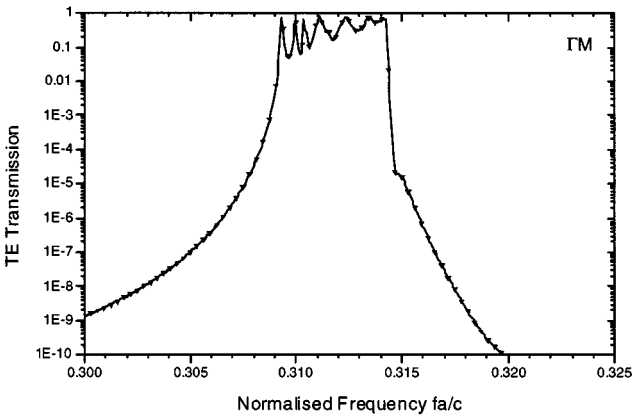

Fig. 5. Closer look at 1 in 3 defects in the ΓM lattice direction. The TE polarized wave transmission response for a superlattice of defects introduced into the lattice by in-filling every third lattice site in the high symmetry directions of the lattice.

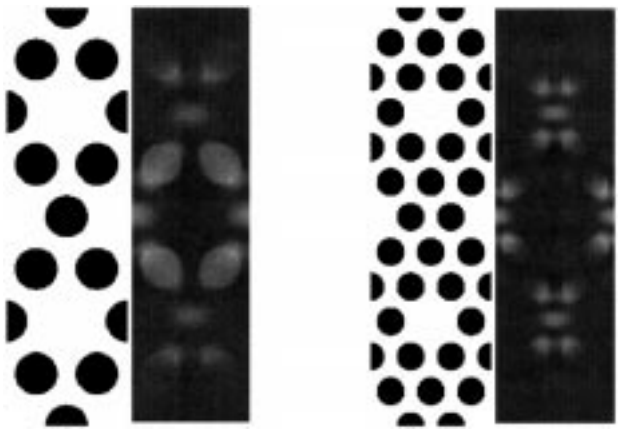

Fig. 7. Field modulus and dielectric distribution. The field modulus shown for the "one in two" and "one in three" superlattices introduced into an otherwise perfect hexagonal crystal as outlined in the caption of Fig. 2. The dielectric profile is also shown so that the position of the defects can be easily ascertained.

B. Superlattice Evolution

The TE transmission response as a function of the superlattice period, expressed as defect neighbor to neighbor distance, is shown in Fig. 6 for transmission through two cells of structure. The plots clearly show convergence of the defect transmission resonance frequency as the distance between the defects increases.

The large difference in the width of the miniband for ΓM incidence between the "one in two" and "one in three" defect superlattices is noteworthy. The miniband formed by the ΓM "one in two" defect lattice is considerably larger than that of the "one in three," or to the same defect superlattice for transmission in the ΓK crystal direction. This means that the defects are coupling strongly to each other. Increasing the distance between defect sites to "one in three" decreases the coupling and the width of the miniband is substantially decreased. This is a finding verified by finite difference time domain calculations, shown in Fig. 7, which show the modulus of the electric field for a normalized fre-

quency of $fa/c = 0.2921$ and $fa/c = 0.3126$ for the "one in two" and "one in three" superlattices respectively. The difference in field localization can be clearly seen between the two cases with stronger coupling in the "one in two" superlattice example.

Both lattice directions show convergence toward a defect resonance frequency of $fa/c = 0.312$ as the distance between defects is increased. The quality factor of the defect state is also improved by increasing the distance between defects resulting in an increased reflectivity between defect sites. This means that for certain applications the quality factor *Q* of the system can be engineered to match either the wanted *Q*, or to increase the coupling efficiency between the PC chip and other emitting components.

V. Conclusion

In summary, we have presented both theoretical and numerical descriptions of coupled defects in PBG crystals. Based on a weak interaction approach, explicit expressions have been derived for the interaction between defects and the influence of perturbations. The actual configuration of the defects, chain, lattice, etc. enters the equations as a linear coupling between neighboring defects. The results have been compared favorably with widely accepted numerical methods, the transfer matrix method, and finite difference time domain method to compare the electromagnetic properties of the structures.

Future devices may benefit greatly from using coupled defects to guide electromagnetic radiation. Bends in coupled-defect chains can be introduced along the crystal's inherent symmetry axis with no insertion loss, i.e., mode mismatch due to bends in straight wave guiding does not occur. The *Q*-factor of the defect state can be tuned to suit the intended application as can the localization frequency by altering the type of defect introduced into the lattice. It is noteworthy that the defects introduced into a lattice need not necessarily be a superlattice themselves, nor involve the complete filling of lattice sites. Chains of defects in a straight line with a periodic pattern will suffice to guide a signal through a PC chip.

Appendix
Derivation of Coupled–Mode Equations for Defects in a Perfect PC

This Appendix derives the equations that describe the evolution of fields attached to defects in a PC. The analysis is general and assumes a three-dimensional (3-D) PC, but can easily be applied to 2-D, or one-dimensional (1-D) crystals. This only affects the dimension of the space where the integrations are performed.

It is assumed that both the electric and magnetic field structures $\vec{E}_0$ and $\vec{H}_0$, and the eigenfrequency ω_0, of the eigenmode of a single defect in an otherwise perfect crystal are known. The influence of other defects is considered as a weak perturbation. Therefore, the field structure of the defect does not change and only the respective amplitude $a(t)$ evolves in time. Hence, the electric $\vec{E}(\vec{r}, t)$ and magnetic $\vec{H}(\vec{r}, t)$ fields attached to the defect are approximated as

$$\vec{E}(\vec{r}, t) = \frac{a(t)}{\sqrt{W_0}}\,\vec{E}_0(\vec{r}) \quad \text{and} \quad \vec{H}(\vec{r}, t) = \frac{a(t)}{\sqrt{W_0}}\,\vec{H}_0(\vec{r}). \tag{A1a}$$

For convenience we have scaled the amplitude a in that way that its squared absolute value corresponds to the actual mode energy. W_0 provides the respective reference to the energy of the field structures used in (A1a) as

$$W_0 = \int d^3\vec{r}\left(\varepsilon_0\varepsilon_R\left|\vec{E}_0\right|^2 + \mu_0\left|\vec{H}_0\right|^2\right)$$

where $\varepsilon_R(\vec{r})$ is the relative dielectric constant, constituting the PC lattice and the defect that is non dispersive in the frequency domain under consideration. We define the unperturbed fields $\vec{E}^{\text{unperturbed}}$ and $\vec{H}^{\text{unperturbed}}$, which represent the true defect mode in the absence of any perturbation as

$$\vec{E}^{\text{unperturbed}}(\vec{r}, t) = \vec{E}_0(\vec{r})\exp(-i\omega_0 t)$$

and

$$\vec{H}^{\text{unperturbed}}(\vec{r}, t) = \vec{H}_0(\vec{r})\exp(-i\omega_0 t). \tag{A1b}$$

We compare these to the real field structures at the defect and evaluate the following expression by applying Maxwell's equations and inserting (A1a) and (A1b)

$$\begin{aligned}
&\operatorname{div}\left(\vec{E}^{\text{unperturbed}^*} \times \vec{H}\right) \\
&\quad = -\mu_0\vec{H}\,\frac{\partial}{\partial t}\,\vec{H}^{\text{unperturbed}^*} - \vec{E}^{\text{unperturbed}^*} \\
&\qquad \cdot \frac{\partial}{\partial t}\left(\varepsilon_0\varepsilon_R\vec{E} + \vec{P}\right) \\
&\quad = -i\,\frac{\omega_0\mu_0}{\sqrt{W_0}}\left|\vec{H}_0\right|^2 a - \frac{\varepsilon_0\varepsilon_R}{\sqrt{W_0}}\left|\vec{E}_0\right|^2\frac{\partial}{\partial t}\,a \\
&\qquad - \vec{E}^{\text{unperturbed}^*}\,\frac{\partial}{\partial t}\,\vec{P}.
\end{aligned} \tag{A2}$$

Any perturbation due to the action of neighboring defects is incorporated into an additional polarization field $\vec{P}(\vec{r}, t)$. Next, we integrate (A2) over the whole space. As nonpropagating modes decay exponentially in space the left-hand side of (A2) vanishes to give

$$\begin{aligned}
0 = \; &-i\omega_0\int d^3\vec{r}\mu_0\left|\vec{H}_0\right|^2 a - \int d^3\vec{r}\varepsilon_0\varepsilon_R\left|\vec{E}_0\right|^2\frac{\partial}{\partial t}\,a \\
&-\sqrt{W_0}\int d^3\vec{r}\vec{E}^{\text{unperturbed}^*}\,\frac{\partial}{\partial t}\,\vec{P}.
\end{aligned} \tag{A3}$$

Next, the magnetic energy of the unperturbed defect mode is transformed, which appears in the first term on the right-hand side of (A3)

$$\begin{aligned}
\int d^3\vec{r}\mu_0\left|\vec{H}_0\right|^2 &= \frac{1}{\omega_0^2\mu_0}\int d^3\vec{r}\left|\operatorname{rot}\vec{E}_0\right|^2 \\
&= \frac{1}{\omega_0^2\mu_0}\int d^3\vec{r}\vec{E}_0^*\operatorname{rot}\operatorname{rot}\vec{E}_0 \\
&= \int d^3\vec{r}\varepsilon_0\varepsilon_R\left|\vec{E}_0\right|^2
\end{aligned} \tag{A4}$$

and find that it is equal to the respective electrical energy. Consequently (A3) can be transformed into an evolution equation of the amplitude of the defect mode as

$$i\frac{\partial}{\partial t}a_i = \omega_0 a - \frac{i\sqrt{W_0}}{\int d^3\vec{r}\varepsilon_0\varepsilon_R\left|\vec{E}_i\right|^2}\int d^3\vec{r}\vec{E}_i^{\text{unperturbed}^*}\frac{\partial}{\partial t}\vec{P}_i \tag{A5}$$

where the polarization appears as the driving term scaled with the mode energy. We have already labeled the amplitude and the polarization with an index i to demonstrate that similar expressions hold for all other defects $i = 1, \ldots, N$.

Now we formulate an explicit expression for the polarization $\vec{P}_i(\vec{r}, t)$, which acts on defect i. This includes the influence of all of the inhomogeneities of the PC lattice, the action of which is not incorporated into the field structures defined in (A1a) and (A1b). Hence, all the fields of neighboring defects and the respective changes of the relative dielectric constants contribute as

$$\vec{P}_i = \frac{\varepsilon_0}{\sqrt{W_0}}\sum_{\substack{j=1\\ j\neq i}}^{N}\left(\sum_{k=1}^{N}\delta\varepsilon_k\right)a_j\vec{E}_j + \frac{\varepsilon_0}{\sqrt{W_0}}\left(\sum_{\substack{k=1\\ k\neq i}}^{N}\delta\varepsilon_k\right)a_i\vec{E}_i. \tag{A6}$$

Before inserting (A6) into (A5), we deal with the time derivative in front of the polarization in (A5). Inspecting (A6), we find that the time evolution of the polarization is entirely determined by that of the field amplitudes oscillating at almost the carrier frequency of the defects ω_0. As long as the power transfer between the defects is slow compared with this fast oscillation the time derivative in (A5) can be replaced by $-i\omega_0$. The final expression now reads as

$$i\frac{\partial}{\partial t}a_i = (\omega_0 - c_{ii})a_i - \sum_{\substack{j=1\\ j\neq i}}^{N}c_{ij}a_j. \tag{A7}$$

The coupling coefficients are given by

$$c_{ij} = \frac{\omega_0}{\int d^3\vec{r}\varepsilon_R\left|\vec{E}_i\right|^2}\int d^3\vec{r}\left(\sum_{k=1}^{N}\delta\varepsilon_k\right)\vec{E}_i^*\vec{E}_j \quad \text{for } i\neq j$$

and

$$c_{ii} = \frac{\omega_0}{\int d^3\vec{r}\varepsilon_R\left|\vec{E}_i\right|^2}\int d^3\vec{r}\left(\sum_{\substack{k=1\\ k\neq i}}^{N}\delta\varepsilon_i\right)\vec{E}_i^*\vec{E}_i. \tag{A8}$$

Note that (A7) accounts for both the interaction of the defects represented by c_{ij}, $i \neq j$ and for the shift of the eigenfrequency introduced by neighboring defects (c_{ii}). Because the electrical components of the field structures of the defect modes can be chosen in such a way that they are real valued, the coupling coefficients are also real. If the defects are well separated and the field distributions attached to the defects decay exponentially in space, small terms in (A8) can be neglected. Particularly, the energy exchange terms can be simplified as

$$c_{ij} \cong \frac{2\varepsilon_0\omega_0}{W_0}\int d^3\vec{r}(\delta\varepsilon_i + \delta\varepsilon_j)\vec{E}_i^*\vec{E}_j, \qquad \text{for } i\neq j.$$

In most cases, the eigenfrequency shift is the same for all defects and can be added to ω_0. However, if small dielectric losses are present, their influence can be incorporated into the polarization $\vec{P}$. Following (A8), one obtains a small imaginary contribution to the eigenfrequency, which introduces a damping.

Real PC systems are finite; therefore, boundaries play an important role. The fields attached to the defect transform from bound states, which decay exponentially into every space direction to leaky modes, which have oscillating tails outside the PC and contribute to either the transmitted or reflected field. Consequently, the eigenfrequency of these leaky defect modes contains a small imaginary part $-i\gamma_i$, which accounts for the decay of the mode amplitude due to radiative losses. The same defect mode can be excited by external radiation allowing for an interaction of the coupled-defect system with its environment. We add these two terms intuitively to the evolution equation (A7) to describe damping and external excitation of defect modes as

$$i\frac{d}{dt}a_i = (\omega_0 - c_{ii} - i\gamma_i)a_i + \hat{\tau}_i a_{\text{in}_i} - \sum_{\substack{i=1\\ i\neq j}}^{N}c_{ij}a_j \tag{A9}$$

where the field a_{in_i} is the amplitude of the incident field at the defect position i, which couples to the defect mode via $\hat{\tau}_i$. Provided that the background transmission of the PC structure vanishes the amplitude of the transmitted field $a_\tau(\vec{r})$ is formally expressed by

$$a_\tau(\vec{r}) = \sum_{i=1}^{N}c_{\tau_i}(\vec{r})a_i \tag{A10}$$

where $c_{\tau_i}(\vec{r})$ describes the field pattern emerging from a single defect toward free space. In case of a regular defect lattice and for a plane-wave excitation (10) yields the contributions to the different diffracted orders of the transmitted field.

REFERENCES

[1] N. Stefanou and A. Modinos, "Impurity bands in photonic insulators," *Phys. Rev. B*, vol. 57, no. 19, pp. 12 127–121 333, May 1998.

[2] A. Yariv, Y. Xu, R. K. Lee, and A. Scherer, "Coupled resonator optical waveguide: A proposal and analysis," *Opt. Lett.*, vol. 24, pp. 711–713, 1999.

[3] M. Bayindir, B. Temelkuran, and E. Ozbay, "Tight-binding description of the coupled defect modes in three-dimensional photonic crystals," *Phys. Rev. Lett.*, vol. 84, no. 10, pp. 2140–2143, Mar. 2000.

[4] ——, "Propagation of photons by hopping: A waveguiding mechanism through localized coupled-cavities in three-dimensional photonic crystals," *Phys. Rev. B, Condens. Matter*, vol. 61, p. R11855, 2000.

[5] M. Bayindir and E. Ozbay, "Heavy photons at coupled-cavity waveguide band edges in a three-dimensional photonic crystal," *Phys. Rev. B, Condens. Matter*, vol. 62, no. 4, pp. R2247–R2250, July 2000.

[6] M. Bayindir, S. Tanriseven, and E. Ozbay, "Propogation of light through localized coupled cavity modes in one-dimensional photonic band gap structures," *Appl. Phys. A, Solids Surf.*, vol. 72, no. 1, pp. 117–119, Jan. 2001.

[7] M. Bayindir, B. Temelkuran, and E. Ozbay, "Photonic crystal based beam splitters," *Appl. Phys. Lett.*, vol. 77, no. 24, pp. 3902–3904, Dec. 2000.

[8] S. Noda, A. Chutinan, and M. Imada, "Trapping and emission of photons by a single defect in a photonic band gap structure," *Nature*, vol. 407, pp. 608–610, October 2000.
[9] J. D. Joannopoulos, R. D. Meade, and J. N. Winn, *Photonic Crystals Molding the Flow of Light*. Princeton, NJ: Princeton Univ. Press, 1995.
[10] A. Mekis, J. C. Chen, I. Kurland, S. Fan, P. R. Villeneuve, and J. D. Joannopoulos, "High transmission through sharp bends in photonic crystal waveguides," *Phys. Rev. Lett.*, vol. 77, p. 3787, 1996.
[11] B. Temelkuran and E. Ozbay, "Experimental demonstration of photonic crystal based waveguides," *Appl. Phys. Lett.*, vol. 74, no. 4, pp. 486–488, Jan. 1999.
[12] G. Tayeb and D. Maystre, "Rigorous theoretical study of finite-size two-dimensional photonic crystals doped by microcavities," *J. Opt. Soc. Amer. A*, vol. 14, p. 3323, 1997.
[13] T. Sondergaard and K. H. Dridi, "Energy flow in photonic crystal waveguides," *Phys. Rev. B, Condens. Matter*, vol. 61, no. 23, pp. 15 688–15 696, June 2000.
[14] J. Yonekura, M. Ikeda, and T. Baba, "Analysis of finite 2-D photonic crystals of columns and lightwave devices using the scattering matrix method," *J. Lightwave Technol.*, vol. 17, pp. 1500–1508, Aug. 1999.
[15] W. Haus, *Waves and Fields in Optoelectronics*. Englewood Cliffs, NJ: Prentice-Hall, 1984.
[16] A. Yariv, *Optical Electronics*, 4 ed. Philadelphia, PA: Saunders, 1991, pp. 519–524.
[17] J. B. Pendry and A. MacKinnon, "Calculation of photon dispersion relations," *Phys. Rev. Lett.*, vol. 69, p. 2772, 1992.
[18] C. M. Soukoulis, Ed., *Photonic Band Gap Materials*, New York: Plenum, 1993.
[19] P. M. Bell, J. B. Pendry, and A. J. Ward, "A program for calculating photonic band structures and transmission coefficients of complex structures," *Comp. Phys. Commun.*, vol. 85, p. 306, 1995.
[20] J. B. Pendry, "Calculating photonic band structure," *J. Phys. Condens. Matter*, pp. 1086–1108, 1996.
[21] J. B. Pendry and P. M. Bell, "Transfer matrix techniques for electromagnetic waves," NATO Adv. Study Inst. Photon. Band Gap Mater., June 1996.
[22] A. J. Ward and J. B. Pendry, "Refraction and geometry in Maxwell's equations," *J. Modern Opt.*, vol. 43, p. 773, 1996.
[23] Translight: A transfer matrix method based program for calculating the transmission and reflection properties of finite thickness photonic crystals, A. L. Reynolds. [Online]. Available: http://www.elec.gla.ac.uk/~areynolds

Andrew L. Reynolds was born in Birmingham, England, in 1974. He received the European Master of Electronics Optoelectronics, M.Eng., and Ph.D. degrees in 1996 and 2000, respectively, from the University of Glasgow, Scotland.

In 1997, he spent one year as a Young Graduate Trainee in the Antenna Section of the European Space Research and Technology Centre (ESTEC), Noordwijk, The Netherlands. His research interests are focused on PBG materials to antenna and optoelectronic applications.

Ulf Peschel was born in Jena, Germany, in October 1964. He received the diploma and the Ph.D. degree in physics from the Friedrich-Schiller-Universität Jena, in 1990 and 1994, respectively.

Since then he has been with the Friedrich Schiller Universität Jena. During 1998 and 1999, he spent one year with the University of Glasgow, U.K. His research interests include microoptics, nonlinear optics, and nonlinear dynamics.

Falk Lederer was born in Tannenbergstual, Germany, in 1948. He received the Diploma degree and Ph.D. degree in physics from the Friedrich-Schiller-Universität Jena, Jena, Germany, in 1972 and 1977, respectively.

He is currently the Head of the Photonics Group, Friedrich-Schiller-Universität Jena. His research interests include nonlinear optics, integrated optics, and optical communications.

Peter John Roberts was born in Dover, England, in 1968. He received the B.A. degree in physics from Oxford University in 1989 and the Ph.D. degree in theoretical condensed matter physics in 1992.

Since then, he has been with the Defence Evaluation and Research Agency (DERA), Malvern, England. His research interests include PBG materials, waveguide, optics, nanowires, statistical optics, and signal processing.

Thomas F. Krauss was born in Rheinbach, Germany, in 1964. He received the Dipl.-Ing. in photographic engineering from the FH Koeln, Germany, in 1989, and the Ph.D. degree in electrical engineering from the University of Glasgow, Scotland, in 1992.

In 1993, he won an EPSRC Research Fellowship in the area of PBGs, thereby initiating a new field at Glasgow University, followed by a Royal Society Research Fellowship in 1995. He is one of the pioneers of waveguide-based, high-index contrast photonic microstructures in semiconductors, and made the first demonstration of 2-D PBG effects at optical wavelengths (1996). In 1997, he spent one year at Caltech and the University of California, Los Angeles, working on photonic crystal light emitters. In March 2000, he moved to St. Andrews University, Scotland, where he is currently establishing a research group and setting up a semiconductor microfabrication laboratory.

Peter J. I. de Maagt (M'88) was born in Pauluspolder, The Netherlands, in 1964. He received the M.Sc. and Ph.D. degrees from Eindhoven University of Technology, Eindhoven, The Netherlands, in 1988 and 1992, respectively, both in electrical engineering.

He is currently with the European Space Research and Technology Centre (ESTEC), European Space Agency, Noordwijk, The Netherlands. His research interests are in the area of millimeter and submillimeter-wave reflector and planar integrated antennas, quasi-optics, PBG antennas, and millimeter- and submillimeter-wave components.